Bioactive collagen-based 3D printed poly (glycerol sebacate) composite scaffold with biomimicking mechanical properties for cartilage defect repair

Yu-Yao Liu[1,2] #, Claudio Intini[3,4,5]#, Marko Dobricic[3,4,5], Fergal J. O'Brien[3,4,5]*, Javier Llorca[1,2]* and Monica Echeverry-Rendon[1]*

[1] IMDEA Materials Institute, 28906 Getafe, Madrid, Spain

[2] Department of Materials Science, Polytechnic University of Madrid/Universidad Politécnica de Madrid, 28904 Madrid, Spain

[3] Tissue Engineering Research Group, Department of Anatomy & Regenerative Medicine, Royal College of Surgeons in Ireland (RCSI), Dublin, Ireland

[4] Trinity Centre for Biomedical Engineering, Trinity College Dublin (TCD), Dublin 2, Ireland

[5] Advanced Materials and Bioengineering Research (AMBER) Centre, RCSI and TCD, Dublin, Ireland

---

# These authors contributed equally to this work.

* Corresponding authors.

E-mail addresses: fjobrien@rcsi.ie (F. J. O'Brien), javier.llorca@imdea.org (J. Llorca) and monica.echeverry@imdea.org (M. Echeverry-Rendon)

Abstract

Cartilage defect repair with optimal efficiency remains a significant challenge due to the limited self-repair capability of native tissues. The development of bioactive scaffolds with biomimicking mechanical properties and degradation rates matched with cartilage regeneration while simultaneously driving chondrogenesis, plays a crucial role in enhancing cartilage defect repair. To this end, a novel composite scaffold with hierarchical porosity was manufactured by incorporating a pro-chondrogenic collagen type I/II-hyaluronic acid (CI/II-HyA) matrix to a 3D-printed poly(glycerol sebacate) (PGS) framework. Based on the mechanical support of PGS framework, the composite scaffold exhibited a compressive modulus of 167.0 kPa, similar to that of native cartilage, as well as excellent fatigue resistance, similar to that of joint tissue. *In vitro* degradation tests demonstrated that the composite scaffold maintained structural, mass, and mechanical stability during the initial cartilage regeneration period of 4 weeks, while degraded linearly over time. *In vitro* biological tests with rat-derived mesenchymal stem cell (MSC) revealed that, the composite scaffold displayed increased cell loading efficiency and improved overall cell viability due to the incorporation of CI/II-HyA matrix. Additionally, it also sustained an effective and high-quality MSC chondrogenesis and abundant *de-novo* cartilage-like matrix deposition up to day 28. Overall, the bioactive composite scaffold with sufficient mechanical support, matched degradation rate with cartilage

regeneration, and effective chondrogenesis stimulation showing great potential to be an ideal candidate for enhancing cartilage defect repair.

Keywords: Poly (glycerol sebacate); Collagen; 3D-printing; Chondrogenesis; Cartilage defect repair.

1. Introduction

Cartilage defects caused by trauma or disease negatively affect the quality of life of over 500 million people worldwide and effective treatments remain a significant challenge in clinical applications in recent 10 years [1,2]. Cartilage tissue is a porous-viscoelastic connective tissue populated by a low density of chondrocytes embedded in a dense extracellular matrix (ECM), substantially limiting their mobility and ability to repair damaged tissue [3,4]. The lack of nerves and blood vessels in its structure remains a big contributing factor that ultimately leads to ineffective cartilage repair with the consequent formation of low-quality hyaline tissue, which is unable to satisfy its function [5–7]. Although traditional surgical treatments consisting of autografts and allografts can be effective on a short-term basis (<5 years), clinical success in the long-term over 5 years is poor and ultimately can lead to full knee arthroplasty or revision surgery in patients [8]. In this regard, tissue engineering (TE) has drawn a lot of attention in recent 20 years, with some cartilage-engineered scaffolds showing promising alternatives [9,10]. Despite some successes in supporting chondrogenesis and cartilage-like matrix formation, most scaffolds still display unmatched mechanical properties and degradation rates with native cartilage, greatly affecting tissue repair efficiency [11]. Consequently, there is an urgent need to develop innovative advanced scaffolds that simultaneously meet the requirements of providing mechanical support for cartilage growth, stimulating chondrogenesis, and maintaining structural and mechanical stability during tissue regeneration.

The combination of the manufacturing technique and the material selection allows the design of scaffolds with suitable properties to fulfil the requirements of tissues. For instance, in 3D-printing technologies, features such as shape design and macro/microstructure can be controlled; complementary, the raw materials provide the overall mechanical properties, biological functionality, and degradation rate of the scaffold [12–14]. To this end, biodegradable synthetic polymers such as poly(caprolactone) (PCL), poly(lactic acid) (PLA), and poly(lactic-co-glycolic acid) (PLGA) with tailored mechanical properties, degradation rates, and ease of processing have been widely used in 3D-printed scaffolds for cartilage TE [15–17]. However, high modulus and inelastic behaviour, slow degradation rates, and acidic degradation products are not conducive to tissue repair and limit their suitability. In this regard, as a biocompatible elastomer, poly(glycerol sebacate)(PGS) with flexible and elastic mechanical behaviour has been considered as a suitable material for cartilage defect repair [18]. You's group used a step-by-step curing process to successfully fabricate 3D-printed porous PGS scaffolds and applied them to tissue engineering

such as heart, bone, and cartilage [19–21]. Depending on the printing parameters and micropore sizes, the elastic modulus of PGS scaffolds can be varied from 150.7 to 239.4 kPa, thus approaching the physiological range of healthy articular cartilage (0.1-2 MPa). Meanwhile, PGS exhibit excellent fatigue resistance under dynamic deformations, which is suitable for joint tissue repair [19,22,23]. However, like most biodegradable synthetic polymers, PGS shows low bioactivity due to the lack of bioactive sites, which limits its applications in biomedical and healthcare applications.

To improve bioactivity, attention has been paid to the functionalization of 3D-printed biodegradable polymer scaffolds by incorporating active biomimetic matrices to obtain biomimetic structures [10,24–27]. In this context, ECM-based materials, such as collagen, are considered good candidates due to their excellent biocompatibility and biodegradability properties, but more importantly, because of their ability to direct cell-binding to the ECM and appropriate matrix deposition [28–31]. A pro-chondrogenic matrix formed by incorporating collagen type II and hyaluronic acid (key articular cartilage ECM components) into a collagen type I has been proved to direct mesenchymal stem cell (MSC) chondrogenesis, thereby leading to enhanced hyaline-like cartilage formation while inhibiting late-stage differentiation events and MSC hypertrophy [32,33]. Furthermore, it has been observed in some animal models (e.g., rabbits, goats, and horses) that when this matrix is incorporated into a multilayered collagen-based scaffold, it exhibits a robust ability to drive efficient, high-quality cartilage repair [34–36]. However, despite some progress, its chondrogenic potential and clinical therapeutic application are only involved in small defects repair, due to the limited mechanical properties. Therefore, it remains a challenge to design scaffolds specifically for larger cartilage defect repair that satisfies the requirements of biomimicking mechanical properties and chondrogenic bioactivity, as well as a degradation rate that matches cartilage regeneration in order to ensure long-term integration and stability.

Herein, this study thus proposes a novel biomimetic composite scaffold with hierarchical porosity by directly incorporating a pro-chondrogenic highly porous collagen type I/II and hyaluronic acid (CI/II-HyA) matrix in a 3D-printed PGS scaffold framework. The porous CI/II-HyA matrix provided the biological cue to stimulate MSC chondrogenesis, while the PGS scaffold provided the mechanical enforcement to support new cartilage tissue growth. The mechanical properties in dry and wet conditions were studied under compression, while cyclic compressions under different deformations were performed simultaneously to evaluate the fatigue resistance property. The structural, mass, and mechanical stability after degradation were conducted by immersion in PBS solution for up to 8 weeks. Finally, the proliferation and differentiation of rat-derived MSCs on the scaffolds were systematically studied for up to 28 days *in vitro* to explore the chondrogenic capacity of these novel scaffolds.

2. Materials and Methods

2.1 Preparation of collagen-based PGS composite scaffold

2.1.1 Preparation of 3D-printing ink

The 3D-printing ink was prepared by mixing PGS prepolymer and sodium chloride particles. Firstly, PGS prepolymer was synthesized through glycerol and sebacic acid polycondensation, as previously described [19]. Glycerol (anhydrous, >99.5%, Sigma-Aldrich, Germany) and sebacic acid (analytical grade, 99%, Sigma-Aldrich, Germany) at a molar ratio of 1:1 were mixed and heated to 120 °C under agitation in a nitrogen atmosphere for 24 h. Then, the pressure was reduced to 2 mbar, and a continuous stirring was conducted at 120 °C for another 24 h to obtain the PGS prepolymer. After this, the PGS prepolymer was dissolved in tetrahydrofuran (THF, anhydrous, 99 %, Sigma-Aldrich, Germany) at a mass/volume ratio 1:5. Next, grided sodium chloride particles (NaCl, 99 %, Sigma-Aldrich, Germany, diameter of 1-75 μm) with a double weight of PGS prepolymer were added to the solution and stirred for 24 h. Finally, the mixture was transferred to a vacuum oven and dried at 50 °C overnight to remove the solvent. The resulting composite was used as the ink for the 3D-printing.

2.1.2 Manufacturing of 3D-printed PGS scaffold

A 3D printer (F40, Direct 3D, Italy) with a screw extrusion system was used to manufacture PGS scaffolds. The ink was placed in the printer installed with a 500 μm nozzle and printed at 50 °C with a moving speed of 10 mm/s and a screw flow percentage of 600 %. Once the system was filled up with the ink, cubic shape samples with a design of a layer thickness of 500 μm, a pore diameter of 1000×1000 μm, and a 0°/90° laying pattern were printed. Then, the obtained samples were placed in a vacuum oven at 100 °C, 0.5 bar for 15 h, and then at 150 °C, 1 bar for 24 h to complete the curing process. The cured scaffolds were soaked in distilled water for 24 h (water was changed 4-6 times) to remove the NaCl particles and then freeze-dried (FreeZone 4.5 Liter -50C Benchtop, Labconco, the United States) at -50 °C under a pressure of 0.2 mbar to get the final PGS scaffolds with high porosity.

2.1.3 Fabrication of the collagen-based PGS composite scaffold

To fabricate the biomimetic composite scaffold, the 3D-printed PGS scaffold was combined with a pro-chondrogenic collagen-based matrix slurry consisting of collagen type I/II and hyaluronic acid (CI/II-HyA) [33]. Briefly, the CI/II-HyA slurry was prepared with a total collagen concentration of 0.5% w/v (collagen I and collagen II at ratio 1:1) and a hyaluronic acid concentration of 0.05% w/v. The 3D-printed PGS scaffold was loaded with 0.3 mL of the previously prepared CI/II-HyA slurry into a stainless-steel tray (dimensions: 9.5 mm diameter and 4 mm height) prior being freeze-dried (Virtis Genesis 25EL, Biopharma, UK) at a constant cooling rate of 1 °C min^{-1} to a final temperature of -20 °C and drying at a pressure of 200

mTorr [37]. Then, the scaffold was punched to get a final dimension of 6 mm diameter and 3 mm height using a commercially available biopsy puncher (Kai Medical, Japan). CI/II-HyA scaffolds without the 3D-printed PGS framework were also fabricated and crosslinked using a dehydrothermally (DHT) crosslinking procedure in a vacuum oven (VacuCell, MMM, Germany) at 105 °C for 24 h under a pressure of 0.05 bar.

2.2 Material Characterization

2.2.1 Composition and structure

The chemical structure of glycerol, sebacic acid, PGS prepolymer, and CI/II-HyA matrix, PGS and composite scaffold were studied by Fourier-transform infrared spectrometer (FT-IR, Nicolet iS50, ThermoFisher). All the spectra were recorded from 1000 - 4000 cm^{-1}. The morphology of CI/II-HyA, PGS, and composite scaffold in top and cross-section view were observed in field emission scanning electron microscope (FESEM, JSM-7800 F, ThermoFisher) with an acceleration voltage of 5.0 kV.

2.2.2 Mechanical characterization

The mechanical properties of original and degraded CI/II-HyA, PGS, and composite scaffolds were evaluated at room temperature by a bioreactor (TC-3F, Ebers, Spain) with a 50 N load cell and compressive grips in dry condition (air) and wet condition (PBS solution). Scaffolds with cylindrical shapes of a diameter of 6 mm and a thickness of 3 mm were used in the tests, while scaffolds for the wet tests were immersed in 0.1M phosphate-buffered saline (PBS, Gibco, UK) overnight before compression. Scaffolds were compressed to a strain of 50% at a speed of 0.1 mm/s, and stress-strain curves were recorded for statistical analysis. Cyclic compressions in dry and wet conditions were carried out by compressing scaffolds to the strain of 10%, 20%, and 40%, respectively, for 10 cycles at the speed of 0.1 mm/s. A minimum of 6 scaffolds were tested for each sample.

2.3 Degradation test

Degradation test was carried out in a 0.1 M PBS solution with a pH value of 7.15 at the physiological temperature of 37 °C, following the ISO 13781 standard [38]. Briefly, CI/II-HyA, PGS, and composite scaffolds with a dimension of 6 mm diameter and 3 mm height were placed respectively into 1.5 mL reaction tubes and filled with PBS at a proportion of at least 30 mL g^{-1} to ensure a complete immersion of scaffolds. Then, scaffolds were placed in an oven at 37 °C and checked every 1 or 2 weeks up to 8 weeks. At each time point, the pH was recorded using a pH meter (Sension + PH3, Hach, USA), and scaffolds were taken out, washed 3 times with deionized water, and freeze-dried at -50 °C under a pressure of 0.2 mbar for 24 h to obtain the change of mass.

2.4 Biological test

2.4.1 Bone-marrow derived mesenchymal stem cells in monolayer

Rat mesenchymal stem cells (MSCs) were cultured in a monolayer prior to being seeded on the scaffolds. Firstly, the cells were isolated from the bone marrow of Wistar rats as previously described, under the approval of the Royal College of Surgeons in Ireland Research Ethics Committee (REC Approval No. 237) [39]. Following, cells from three separate pools of donors were expanded and cultured in monolayer onto T-175 (175 cm^2 growth area) flasks under normoxic cell culture conditions (37 °C, 5 % CO_2, and 21 % O_2). The culture expansion media included high-glucose Dulbecco's modified Eagle's medium (DMEM) (Sigma-Aldrich, Ireland) supplemented with 10% fetal bovine serum (FBS), 100 U mL^{-1} penicillin/streptomycin, 1% L-glutamine, 1% Glutamax and 1% non-essential amino acids (components were supplied by ThermoFisher Scientific, Ireland, unless otherwise specified). Once 70% confluent, cells were passaged using trypsin ethylenediaminetetraacetic acid (EDTA, Sigma-Aldrich, Ireland) and cultured on the scaffolds between passage number 3 and 5.

2.4.2 Culture of MSCs on scaffolds

Rat MSCs were trypsinized from culture flasks and counted to obtain a density of 5×10^5 cells per scaffold in a total volume of 70 µL. Prior to cell seeding, scaffolds were initially pre-hydrated with 2 mL per scaffold of ethanol 70% and PBS (Sigma-Aldrich, Ireland) for 30 min each and placed in 24 well-plates. Then, the scaffolds were seeded with 35 µL of the cell suspension first pipetted onto one side of each scaffold, before incubating for 30 min (37 °C, 5 % CO_2, 21 % O_2). Subsequently, the scaffolds were turned and cultured with the remaining 35 µL of cell suspension pipetted on the other side. Following 30 min incubation, scaffolds were cultured with 2 mL of culture expansion media for 24 h. The culture expansion media was then replaced with 2 mL of chondrogenic culture media including high-glucose DMEM with 50 µg mL^{-1} ascorbic acid, 40 µg mL^{-1} proline, 100 nM dexamethasone, 1×ITS, and 0.11 mg mL^{-1} sodium pyruvate and 20 ng mL^{-1} human TGF-β3 (Prospec, Israel) (components were supplied by ThermoFisher Scientific, Ireland, unless otherwise specified). Cell seeding efficiency was calculated by dividing the effective number of cells seeded on the scaffold (total number of cells seeded per scaffold minus the leftover cells attached at the bottom of the well) by the total amount of cells, as shown in **Figure S1**. The cell-seeded scaffolds were incubated for 28 days, with media changed twice weekly.

2.4.3 Cellular metabolic activity assay

An AlamarBlue assay (ThermoFisher Scientific, Ireland) was conducted to measure the metabolic activity of the cells within the scaffolds. Scaffolds were initially washed in PBS twice and later cultured in fresh chondrogenic media containing 10% AlamarBlue viability reagent at 37 °C for 1 h. A spectrophotometer

(Victor2 D, Wallac, Boston, MA, USA) with an excitation wavelength of 550 nm and an emission wavelength of 590 nm was used to read the resulting fluorescence level. Chondrogenic media containing 10% AlamarBlue were used as a blank sample, subtracted from the experimental readings to eliminate background fluorescence. The cellular metabolic activity of cells grown on scaffolds at days 0, 3, 7, 15, 21, and 28 was measured.

2.4.4 DNA quantification and sulfated glycosaminoglycan (sGAG) quantification

Scaffolds were washed in PBS and digested in a papain enzyme solution prepared with 0.5 M EDTA, cysteine-HCl, and 1mg mL^{-1} papain enzyme (Carica papaya, Sigma-Aldrich, Ireland) at 60 °C for 12 h. The DNA concentration of cells grown on the scaffolds was determined using a Quant-iTTM PicoGreen® dsDNA assay kit (Invitrogen, UK). The sulfated glycosaminoglycan (sGAG) content within the scaffolds was also measured using Blyscan sulfated glycosaminoglycan assay kit (Biocolor Life Sciences, UK). The DNA and sGAG contents for each scaffold were determined using a standard curve at day 28 as per the manufacturer's instructions.

2.4.5 Histological analysis of cellular infiltration and sGAG distribution

Histological staining protocols were used to further evaluate cellular infiltration and sGAG distribution within the scaffolds. Scaffolds were formalin-fixed for 1 h, treated with 1 mL of 15% sucrose for 2 h and 30% sucrose overnight, embedded in OCT (Fisher-Scientific, Ireland), and transversally sectioned at various depths on a cryostat (Leica RM 2255, Leica, Germany) to give 10 μm thick sections. These sections were mounted on PolysineTM glass slides (Fisher-Scientific, Ireland) and stained for Alcian blue (Sigma-Aldrich, Ireland), which stains sGAG blue, and nuclear fast red, which stains the cell nuclei red. The sections were successively imaged at several magnifications using a Leica DMIL microscope (Leica Microsystems, Switzerland).

2.4.6 Gene expression analysis

Quantitative reverse transcriptase polymerase chain reaction (qRT-PCR) was performed to determine the expression of specific genetic markers associated with chondrogenic lineage (Table 1). The total RNA was isolated from the cells within the scaffolds using an RNeasy kit (Qiagen, UK) and reverse transcribed to cDNA at a final concentration of 2.5 ng μL^{-1} using a QuantiTect reverse transcription kit (Qiagen, UK) on a thermal cycler (Mastercycler Personal, Eppendorf, UK). A QuantiTect SYBR Green PCR kit (Qiagen, UK) was used to run qRT-PCR reactions on a 7500 real-time PCR System (Applied Biosystems, UK) as

previously described[40]. The relative expression of mRNA was calculated using the delta-delta Ct (ΔΔCt) method, where delta Ct (ΔCt) was the value obtained by subtracting the cycle threshold value (Ct) of a house-keeping gene from the Ct value of target mRNAs: aggrecan (*ACAN*), collagen type II alpha 1 chain (*COL2A1*) and collagen type I alpha 1 chain (*COL1A1*). The amount of target mRNA relative to the housekeeping gene was normalized to a calibrator sample to generate ΔΔCt. This was then converted to a fold increase in expression using the formula: Fold increase = $2^{-(\Delta\Delta Ct)}$. 18S ribosomal RNA (*18S*) was used as the housekeeping gene.

Table 1. List of gene transcripts analyzed by qRT-PCR. Qiagen QuantiTect validated primers used to analyze the expression levels of target genes.

Target gene	Catalogue code	Target gene reference
Collagen type 1 α1 chain (COL1A1)	QT01081059	Rn_Col1a1_1_SG
Collagen type 2 α1 chain (COL2A1)	QT01084118	Rn_Col2a1_1_SG
Aggrecan (ACAN)	QT00189518	Rn_Acan_1_SG
18S ribosomal RNA (18S)	QT02589300	Rn_Rn18s_1_SG

2.5 Statistical analysis

All the data were recorded as mean ± standard deviation unless stated otherwise. Each experiment was carried out for at least triplicate samples. Statistical analysis was carried out using Origin software (2021b, OriginLab, Northampton, Massachusetts, USA) and GraphPad Prism (GraphPad Software 10.2.0, California USA) using a general linear model one-way analysis of variance (ANOVA) with Fisher's LSD test analysis performed for multiple comparisons. p-values less than or equal to 0.05 ($p \leq 0.05$) were considered statistically significant. * Denotes $p \leq 0.05$, **$p \leq 0.01$, ***$p \leq 0.001$ and ****$p \leq 0.0001$.

Results

3.1 The composite scaffold displayed a well-integrated structure and hierarchical porosity

The complete process of manufacturing, functionalization and evaluation of the material is summarized in **Scheme 1**. After the manufacturing of the samples, FT-IR spectroscopy was used to identify the curing reaction. As shown in **Figure 1a**, in the PGS prepolymer, the absence of the characteristic absorption at

1230 cm^{-1} related to -C-O- in the carboxyl group from sebacic acid, and the weakness of absorption at 3291 cm^{-1} corresponding to the -OH group in glycerol both demonstrate the consumption of monomers during the reaction. Furthermore, the characteristic absorption of -CH_2- in glycerol (2869 cm^{-1} and 2932 cm^{-1}) and -C=O- in sebacic acid (1686 cm^{-1}) both appear in the final PGS scaffold [23], indicating successful curing.

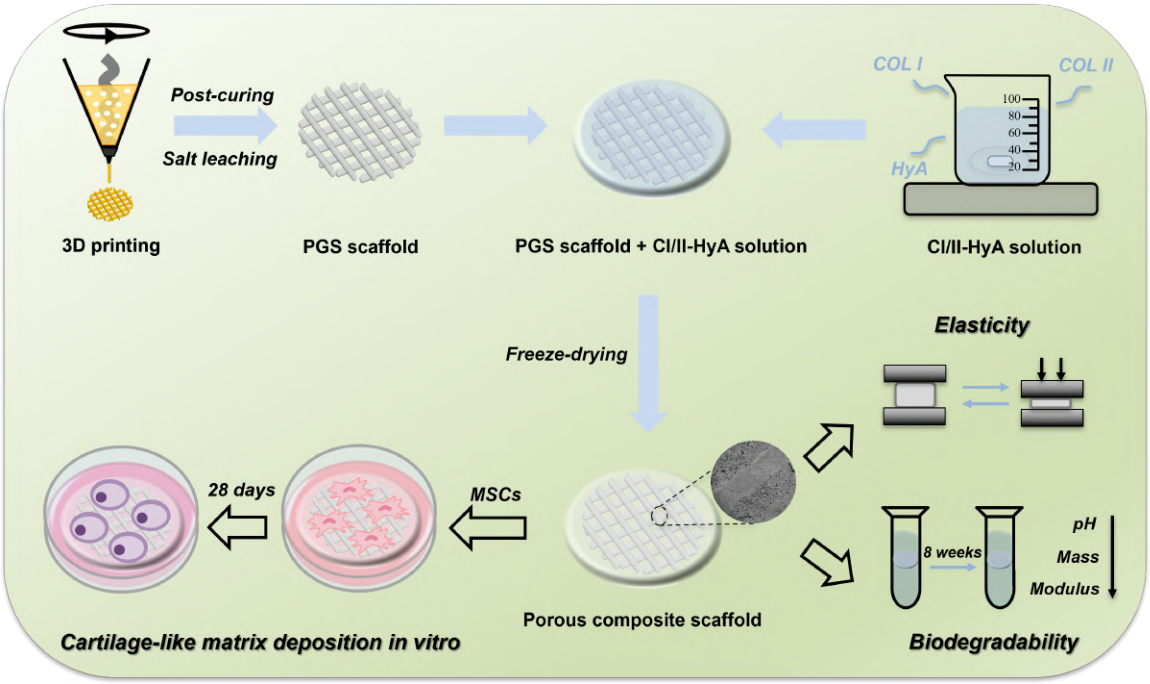

Scheme 1. The fabrication and application of composite scaffold manufactured from a 3D-printed PGS framework and a collagen type I/II-hyaluronic acid (CI/II-HyA) matrix

The composite scaffold was obtained by soaking the PGS scaffold in the mixed solution of collagen type I/type II (total collagen concentration of 0.5% w/v at ratio 1:1) and hyaluronic acid (HyA) at a concentration of 0.05% w/v prior to being freeze-dried to a final temperature of -20 °C. The mass fraction of collagen content in the composite scaffold was determined as 16.54 ± 6.04 %. Besides, it can be observed from the FT-IR spectrum in **Figure 1b** that two specific absorption peaks at 1648 cm^{-1} and 1542 cm^{-1} related to the amide I band and amide II bond in collagen occur in composite compared with the PGS, indicating the successful incorporation.

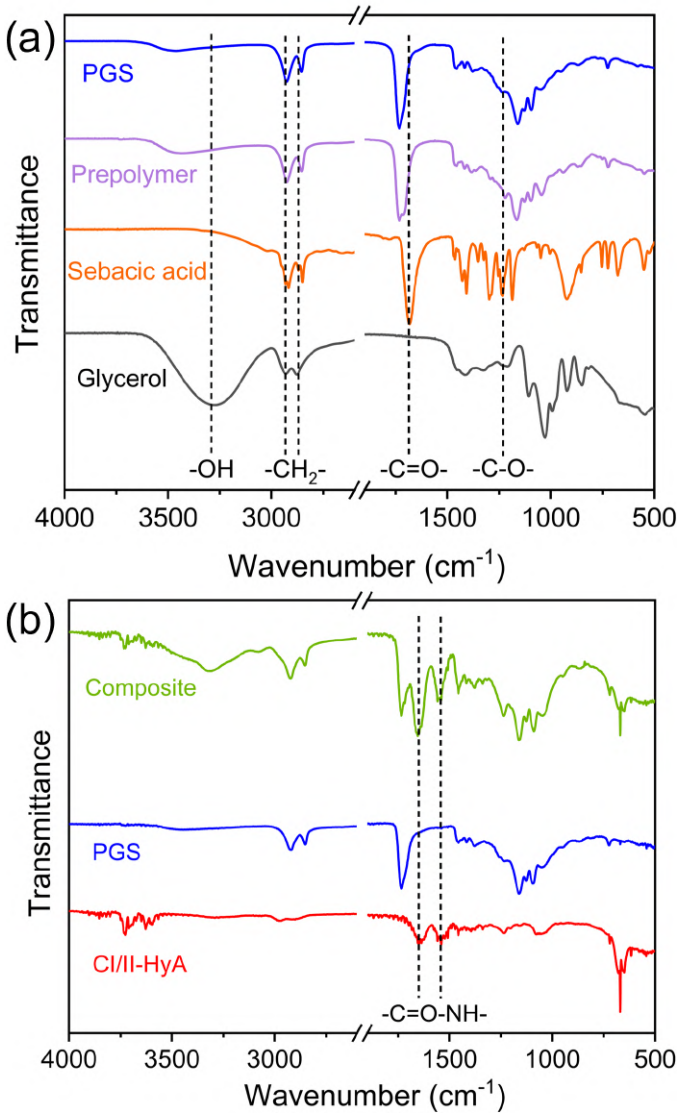

Figure 1. FT-IR spectrum of (a) glycerol, sebacic acid, PGS prepolymer and PGS, and (b) CI/II-HyA, PGS and composite scaffolds

Figure 2 further displays the morphology of CI/II-HyA, PGS, and composite scaffolds. CI/II-HyA scaffold exhibits a fluffy porous structure with a pore size of 155 ± 5 µm and a porosity of 99 % formed through the multiple freeze-drying procedure [33]. 3D-printed PGS scaffold presents an interconnected multi-layer structure, in which the filaments exhibit a homogeneous cylindrical shape with an average diameter of 550 ± 23 µm, and the average gap size between the filaments is 778 ± 34 µm. High microporosity caused by NaCl leaching appears on the surface and inside of PGS filaments, making the overall PGS scaffold show a hierarchical porosity. Additionally, it can be seen in the composite scaffold that the porous collagen matrix is firmly coated on the surface of the porous PGS filaments and fill the printed pores of the PGS scaffold. After incorporation, PGS framework maintained a good spatial structure without filaments deformation and

collapse, and the internal microporous structure was also maintained. These results indicate that the fabrication of the biomimetic composite scaffold with hierarchical porosity was successfully achieved.

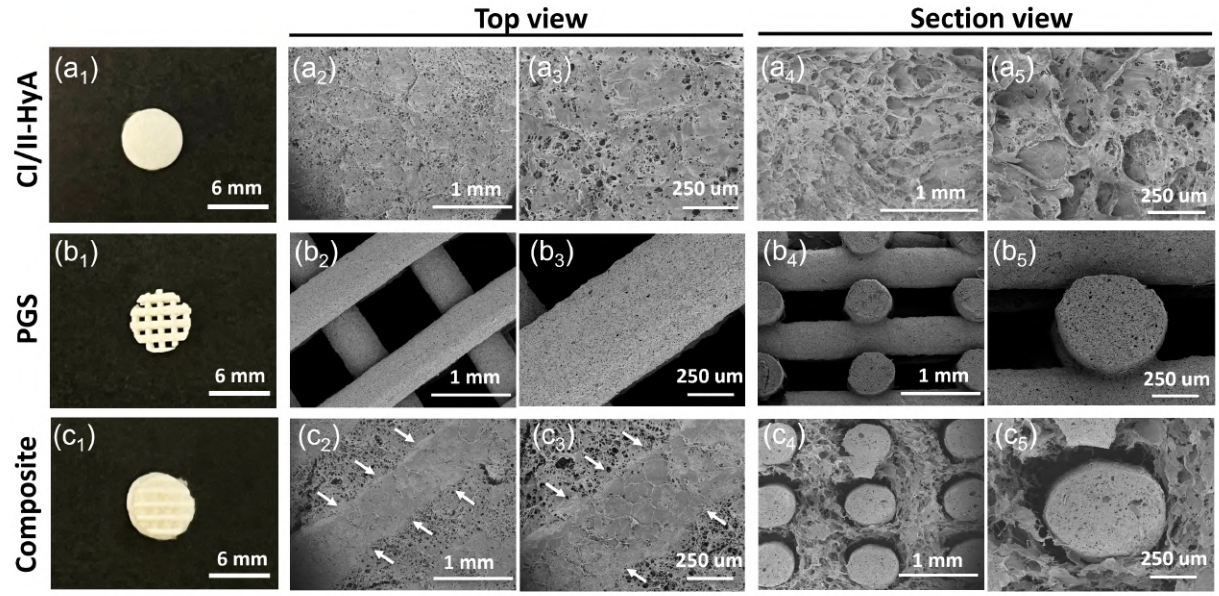

Figure 2. The digital images and SEM images of (a)CI/II-HyA, (b)PGS, (c)composite scaffolds under the top view and section view

3.2 The composite scaffold exhibited high elasticity and fatigue resistance both in dry and wet conditions

The mechanical properties of CI/II-HyA, PGS and composite scaffold were tested through compression and cyclic compression tests under air (dry) and PBS solution (wet) conditions. The incorporation of CI/II-HyA matrix significantly enhanced the mechanical properties of the PGS framework in dry conditions. The compressive modulus of the composite scaffold was 167.0 kPa, which is twice that of the PGS scaffold with a modulus of 80.0 kPa, while the modulus of the CI/II-HyA scaffold was 10.8 kPa. In the PBS solution, the compressive modulus of the composite scaffold was reduced to 45.22 kPa, which was close to that of the PGS scaffold (35.74 kPa), as shown in **Figure 3 and Table 2**. In addition, cyclic compression tests under dynamic strains of 10%, 20%, and 40% show that PGS and composite scaffolds exhibit good elasticity and excellent fatigue resistance under dry and wet conditions (**Figure 4**). Both scaffolds show a complete elastic recovery at low strains of 10% and 20%, while some hysteresis was observed at a high strain of 40%. Among them, the composite scaffold shows more severe hysteresis under high strain in wet conditions.

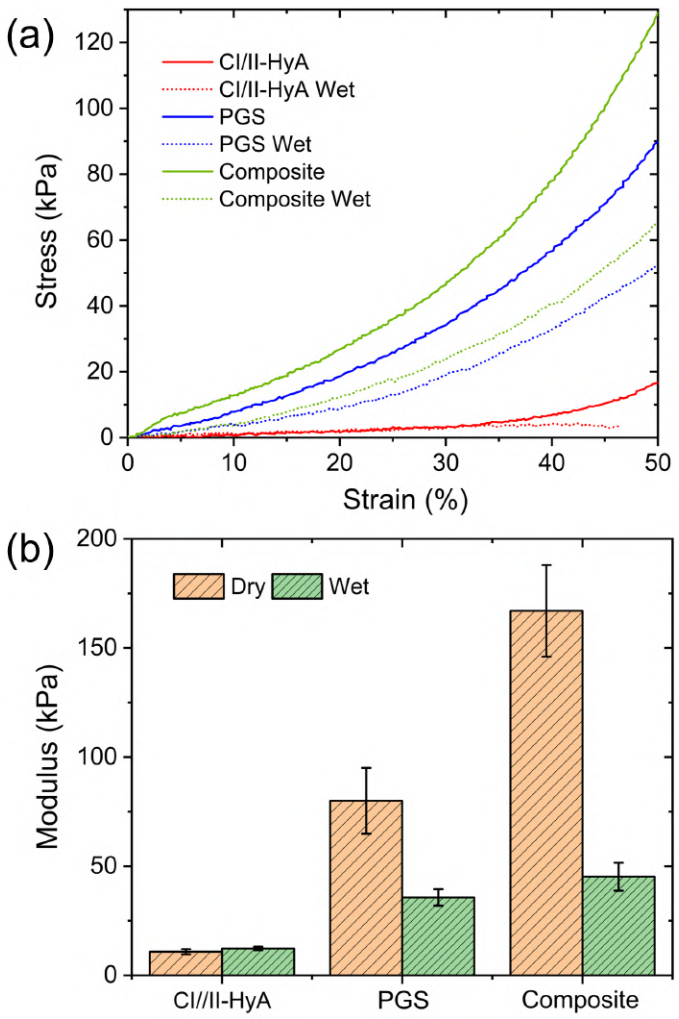

Figure 3. (a) Stress-strain curves and (b) compressive modulus of CI/II-HyA, PGS, and composite scaffold in dry and wet conditions

Table 2 The compressive parameters of CI/II-HyA, PGS and composite scaffolds in dry and wet conditions

Sample	Compressive modulus (kPa)	Compressive stress (kPa)
CI/II-HyA	10.8 ± 1.2	12.6 ± 0.1
CI/II-HyA Wet	12.3 ± 0.8	5.7 ± 0.5
PGS	80.0 ± 15.1	104.4 ± 15.8
PGS Wet	35.7 ± 3.8	60.4 ± 7.0
Composite	167.0 ± 21.0	121.4 ± 8.4
Composite Wet	45.2 ± 6.4	56.7 ± 7.4

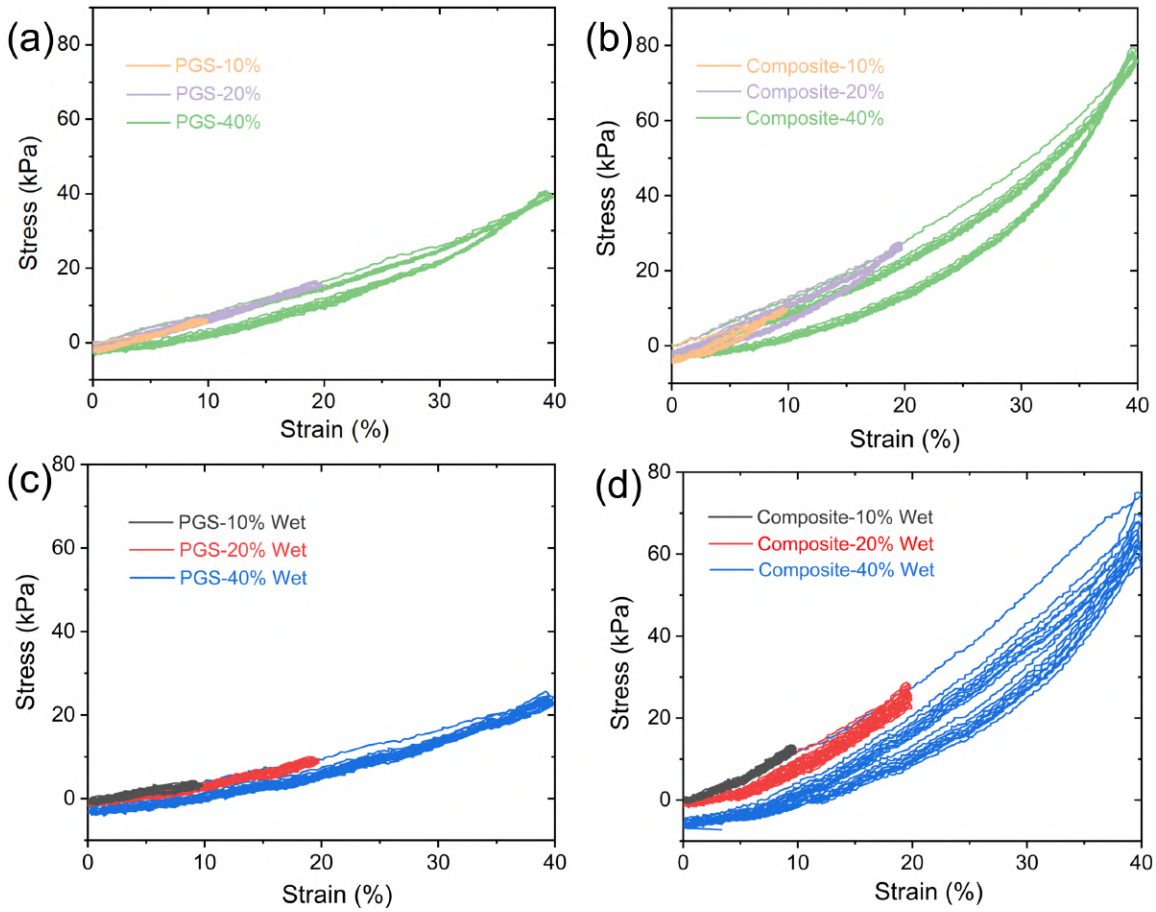

Figure 4. Cyclic compression tests with strains of 10%, 20%, and 40% of (a) PGS scaffold in dry condition, (b) PGS scaffold in wet condition, (c) Composite scaffold in dry condition, and (d) Composite scaffold in wet condition

3.3 Structural, mass, and mechanical stability was maintained in the composite scaffold during the degradation of 8 weeks *in vitro*

The degradation behaviour of CI/II-HyA, PGS, and composite scaffolds was measured *in vitro* at 37 °C in PBS solution for 8 weeks. During the degradation, all scaffolds showed shape integrity without any damage (**Figure S2**) and mass retention with mass losses of 48.52%, 92.51%, and 94.51%, for CI/II-HyA, PGS and composite scaffolds, respectively (**Figure 5a**). In addition, the real-time pH monitoring results presented that the pH value decreased slightly over time. Among them, the composite scaffold showed a linear degradation rate similar to PGS (**Figure 5b**). More importantly, the compressive modulus of PGS and composite scaffolds remained unchanged after 4 weeks of degradation while gradually decreasing after 8 weeks, but the compressive stress decreased significantly with time (**Figure 5c, 5d and Table S1, S2**). Besides, the elasticity and fatigue resistance of both scaffolds were well reflected without any destruction during the time of degradation (**Figure S3**).

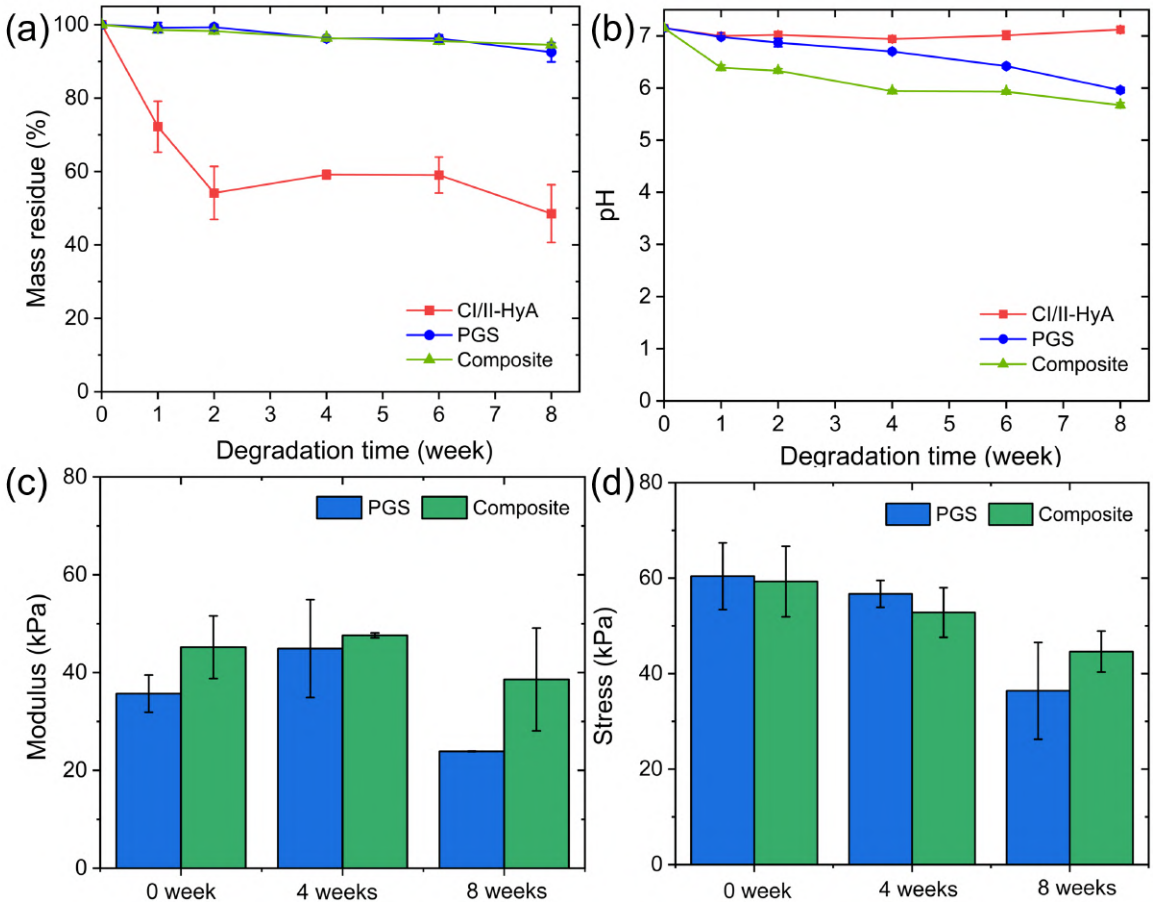

Figure 5. (a) mass residue, (b) pH change, (c) compressive modulus change, and (d) compressive stress change of CI/II-HyA, PGS, and composite scaffolds after degradation with time

3.4 All scaffolds sustained MSC viability up to day 28, with the composite scaffold having the highest DNA levels

The capability of the scaffolds to support cellular viability and growth was evaluated to assess biocompatibility. Biochemical assays revealed that all scaffold variants sustained cellular metabolic activity *in vitro* up to day 28, with the composite scaffolds showing the highest levels of DNA (**Figure 6**). Specifically, all scaffolds resulted in equal cellular metabolic activity at day 28, though PGS and composite scaffolds showed significantly increased cellular metabolic activity at days 7 and 15, compared to the CI/II-HyA scaffold ($p \leq 0.0001$) (**Figure 6a**). However, despite similar metabolic activity was observed between groups at day 28, the composite scaffold possessed the highest overall DNA content level (3.93 µg), compared to CI/II-HyA (2.07 µg) ($p \leq 0.001$) and PGS (1.03 µg) ($p \leq 0.0001$) scaffolds (**Figure 6b**). Furthermore, the DNA levels of the composite scaffold were significantly increased compared to the PGS

scaffold of donors 1 and 2. Although CI/II-HyA scaffold had lower DNA levels than composite scaffolds, they resulted in a significant increase in overall DNA level, compared to PGS scaffold ($p \leq 0.05$).

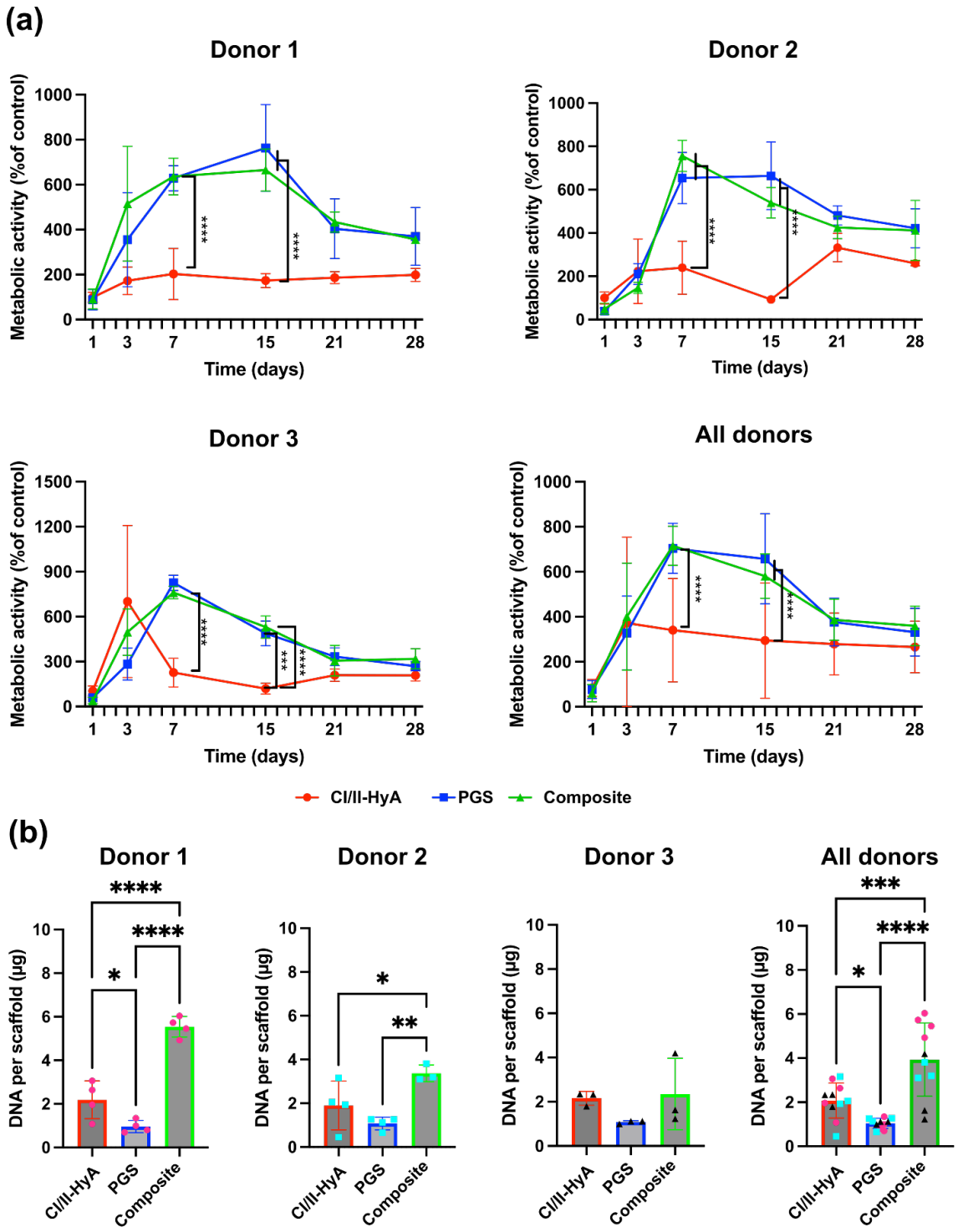

Figure 6. (a) Cellular metabolic activity (normalized to CI/II-HyA scaffolds at 0 day) after 0, 3, 7, 15, 21 and 28 days and (b) DNA content per scaffold after 28 days of CI/II-HyA, PGS and composite scaffolds in culture. Data shown represent the mean from three individual rat MSC donors $n \geq 3$ (unless indicated differently)

3.5 All scaffolds sustained effective MSC chondrogenesis, with up-regulated COL2A1 expression from the composite scaffold

To assess the capability of the scaffolds to sustain effective MSC chondrogenic differentiation, the expression of key genetic markers typically associated with accurate chondrogenesis was investigated. All scaffold variants sustained overall gene expression of Collagen I (*COL1A1*), Collagen 2 (*COL2A1*) and Aggrecan (*ACAN*) of MSC at day 28, thus indicating the ability of these scaffolds to support effective MSC chondrogenic differentiation (**Figure 7**). Interestingly, the composite scaffold displayed significantly higher *COL2A1* compared to CI/II-HyA scaffold ($p \leq 0.05$), demonstrating potential for the composite scaffold to enhance chondrogenesis. Specifically, *COL2A1* gene expression was significantly upregulated in composite scaffold compared to CI/II-HyA scaffold in two individual donors, respectively, donors 1 ($p \leq 0.01$) and 3 ($p \leq 0.05$). Moreover, although it was not significant when compared to the other groups, the composite scaffold also displayed the highest *ACAN* expression at day 28.

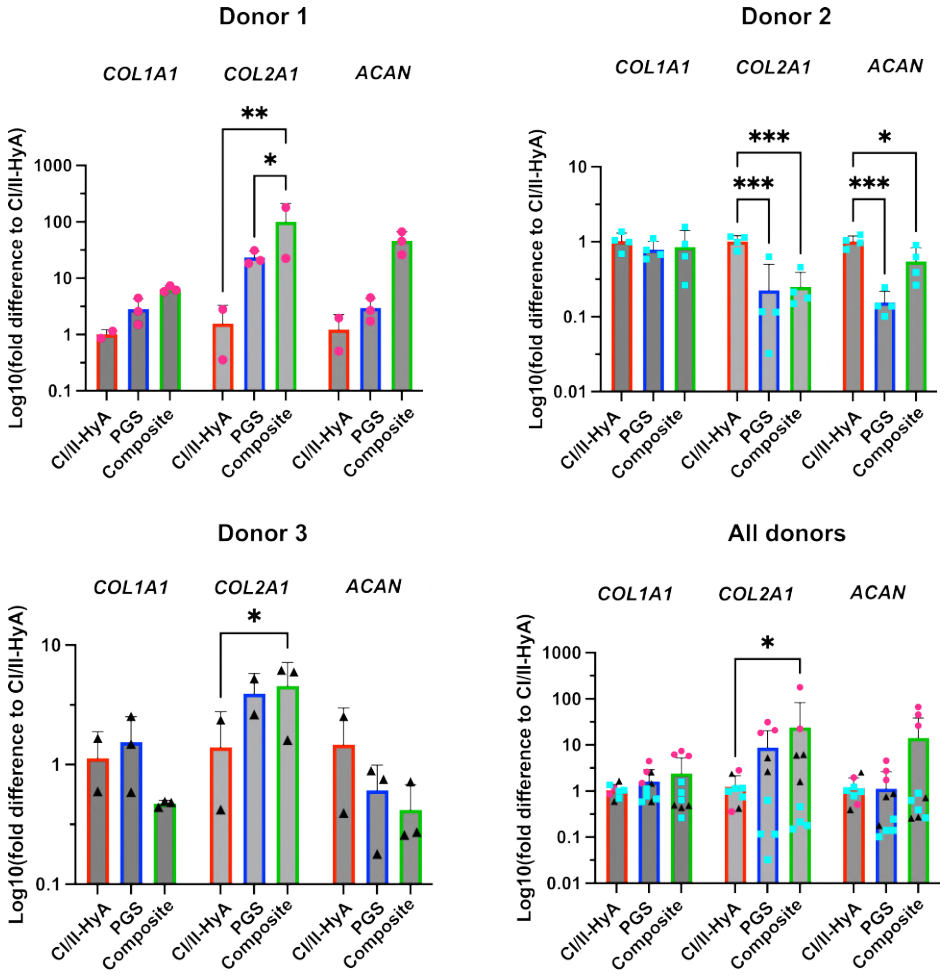

Figure 7. Expression of chondrogenic genes *COL1A1*, *ACAN*, and *COL2A1* of MSC on CI/II-HyA, PGS and composite scaffolds after 28 days in culture. Data shown represent the mean from three individual rat MSC donors $n \geq 3$ (unless indicated differently).

3.6 The composite scaffold supported improved cartilage-like matrix deposition

The ability of the scaffolds to induce cartilage-like matrix formation *in vitro* was then studied by sGAG deposition and histology assessment. All scaffold variants sustained sGAG deposition by MSCs at day 28. The composite scaffolds displayed the highest overall levels of sGAG per scaffold (2.70 µg/mL) (**Figure 8**), which was significantly higher compared to PGS scaffold with a level of 1.63 µg/mL ($p \leq 0.01$). Specifically, the composite scaffold supported significantly increased sGAG quantities compared to PGS scaffold with donors 1 ($p \leq 0.05$) and 3 ($p \leq 0.01$), as well as CI/II-HyA scaffold with donor 3 ($p \leq 0.05$).

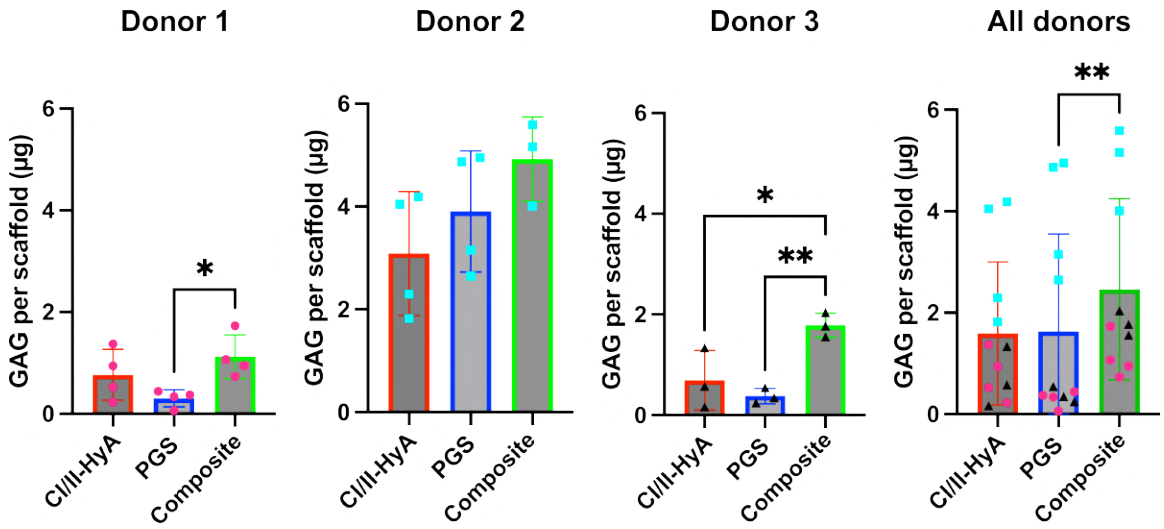

Figure 8. Overall sGAG content on CI/II-HyA, PGS and composite scaffold after 28 days in culture. Data shown represent the mean from three individual rat MSC donors $n \geq 3$ (unless indicated differently).

Furthermore, histological analysis was performed and analysed to qualitatively assess the ability of these scaffolds to sustain effective MSC migration and cartilage-like matrix distribution in the scaffolds. Histological analysis confirmed sGAG presence in all scaffold groups at day 28 (**Figure 9**). CI/II-HyA and composite scaffolds displayed more abundant and homogenous sGAG distribution compared to PGS scaffold. In parallel, a more homogenous cellular infiltration and migration throughout the matrices was also observed in CI/II-HyA and composite scaffolds in comparison to the PGS scaffold.

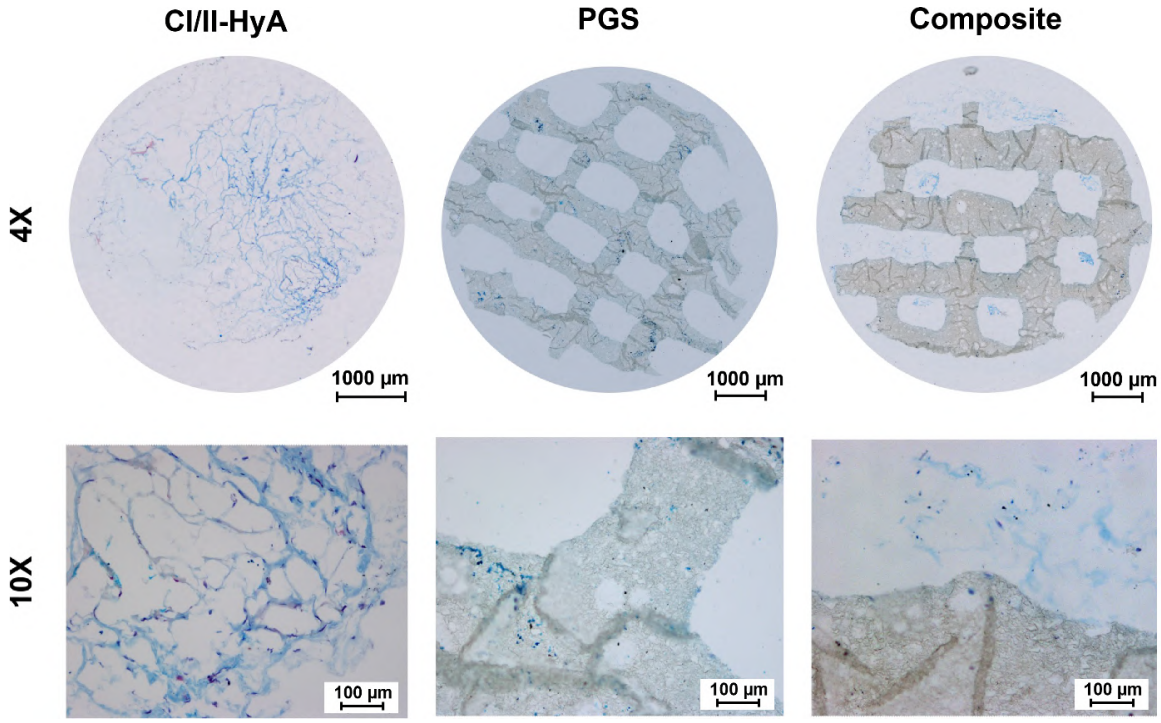

Figure 9. Representative histological images of MSC-seeded scaffolds stained with alcian blue after 28 days in culture. The histological images were collected for scaffolds seeded with rat MSCs from donors 1, 2 and 3. Scale bar represents 1000 µm and 100 µm length for the 4X and 10X magnification, respectively.

4. Discussion

Therapeutic options for efficient cartilage repair are limited due to the poor self-repair ability of native cartilage. Tissue engineering offers a promising alternative for tissue replacement, particularly through the development of scaffolds that combine necessary mechanical properties and appropriate degradation rates, while promoting effective tissue regeneration. To contribute to this field, an innovative composite scaffold with a hierarchical porosity was developed, in which a pre-chondrogenic CI/II-HyA matrix served as a biological cue to stimulate MSC chondrogenesis, while an elastic 3D-printed PGS scaffold served as mechanical enforcement to support cartilage growth. Following this rationale, it is demonstrated that the newly developed composite scaffold can effectively enhance the cartilage repair efficiency in terms of architecture, mechanical properties, degradation rate, and MSC chondrogenesis, showing great promise as an attractive "off-the-shelf" scaffold biomaterial to enhance cartilage defect repair in the clinic.

As a first very notable achievement, the composite scaffold was successfully manufactured with a hierarchical porosity between the porous collagen type I/II-hyaluronic acid matrix and the PGS filaments, which demonstrated both good integration and spatial structure. SEM analysis revealed that the composite scaffolds had an interconnected multi-layer structure, in which the filaments exhibit a homogeneous

cylindrical shape with the porous CI/II-HyA matrix firmly coated on the surface of the porous PGS filaments. Architecturally, the development of these highly porous scaffolds is crucial in cartilage TE to ensure an appropriate nutrient-waste exchange for cell populations colonized on biomaterials, ultimately biologically satisfying their function in a long-term culture environment [41]. Additionally, porosity is important to mimic the viscoelastic behaviours of tissues, which is related to the lubrication and deformation of cartilage [42]. The dimension of the pores in the scaffold is another major feature that can impact cellular behaviour, dictating different MSC responses to migration and chondrogenesis [43]. To this end, the 3D-printed PGS scaffold (with a macro pore size of 778 μm) has been functionalized with a pro-chondrogenic collagen-based (CI/II-HyA) matrix, which has previously been shown to possess the optimal architectural features to facilitate a robust MSC chondrogenesis and cartilage-like formation. Previous research [33] has shown that this kind of collagen-based matrix with an optimal pore size of 155 μm and a highly interconnected porous network of 99% has the ability to facilitate abundant cellular infiltration and viability up to day 28 when tested *in vitro* with rat-derived MSCs. In this study, when this CI/II-HyA matrix was incorporated to the PGS scaffold, it is demonstrated to possess comparable architecture features in terms of porosity and pore size to what was previously found, thus highlighting the successful integration of the pro-chondrogenic matrix to the PGS filaments.

The composite scaffold exhibited adapted elasticity and excellent fatigue resistance under dynamic compression conditions, suitable for use in the cartilage environment under frequent deformation. Notably, after incorporating the CI/II-HyA matrix, the compressive modulus of the composite scaffold in dry conditions was greatly improved due to hydrogen bond interactions in the collagen molecular chain, reaching 167.0 kPa, which is within the modulus range of native cartilage (100-2000 kPa) [44]. While in wet conditions, the modulus of the composite scaffold decreased to 45.22 kPa, similar to that of the PGS scaffold. It demonstrated that although the incorporation of a collagen-based matrix improved the mechanical properties, the PGS scaffold is still the main provider of mechanical support in the composite scaffold. Furthermore, studies [45,46] have shown that during daily physiological activities, the amount of cartilage deformation caused by force is about 10%-20% of its height, depending on the distribution. When articular cartilage undergoes vigorous exercise, its deformation range can be as high as 40%, especially in joint tissues [47,48]. Consequently, developing scaffolds capable of processing adapted elasticity is another important aspect to consider guaranteeing mechanical features that recapitulate cartilage healthy physiological conditions. However, PCL, PLA, and other materials are widely used as the framework to fabricate 3D-printed cartilage scaffolds. While ideally, these materials would enhance cartilage tissue repair under modifications, most of them lack high elasticity[49]. Interestingly, as the mechanical support in the composite scaffold, PGS exhibited elastic recovery under dynamic cyclic compression conditions

of 10%, 20%, and 40%, regardless of dry or wet conditions, indicating its excellent fatigue resistance. Following incorporation into the CI/II-HyA matrix, the composite scaffolds maintained fatigue resistance similar to the PGS scaffold. Therefore, the novel composite scaffold offering mechanical support similar to those of native cartilage shows strong promise in facilitating an effective and enhanced cartilage repair *in vivo*.

Another important characteristic of successful cartilage-engineered constructs is to possess a degradation rate that matches the regeneration rate of native tissues. Therefore, the degradation behaviour of CI/II-HyA, PGS, and composite scaffold in PBS solution at a physiological temperature of 37 °C for 8 weeks was investigated. Results have shown that PGS and composite scaffolds maintained structural, mass, and mechanical integrity within 4 weeks, which matches the speed of MSC chondrogenesis and cartilage-like formation *in vitro*, while CI/II-HyA scaffolds showed a rapid decrease, which lost almost half of its mass in the same period. This is because the PGS framework not only provides mechanical support but also helps to protect against the loss of the collagen-based matrix. Meanwhile, in the composite scaffold, the PGS filaments were firmly surrounded by a collagen-based matrix, limiting the degradation of the PGS framework, which can be proved by the slower liner degradation tendency caused by surface erosion of the composite scaffold than PGS only. It solves the problem of the fast degradation rate of PGS to a certain extent, making it more matched with cartilage regeneration [50]. Additionally, after 8 weeks, the mechanical properties of these scaffolds all showed decreasing, and the tendency of pH and mass kept dropping gradually with time, meeting the requirements of the biodegradable scaffolds in TE. Therefore, the combination of CI/II-HyA matrix and PGS framework shows a syncretic effect on the degradation control, endowing the composite scaffold with a perfect degradation rate matched cartilage tissue regeneration.

Biologically, the composite scaffold demonstrated robust and efficient MSC chondrogenic differentiation, which translated to improved overall cartilage-like matrix formation at day 28 *in vitro*. The novel composite scaffold promoted the highest levels of DNA and sGAG compared to the other groups. In addition to the major mechanical reinforcement provided by the 3D-printed PGS filaments, the PGS framework also supported the porous pro-chondrogenic collagen matrix, thus benefiting the overall construct to obtain an increased cellular proliferation and matrix deposition. These findings are comparable with studies related to cartilage-engineered scaffolds that incorporated bioactive matrices such as alginate/agarose/collagen or hyaluronic acid into 3D-printed frameworks such as PCL and PLA [26,51,52]. It is possible to hypothesize that, while the porous collagen-based matrix ensured adequate cell attachment, migration, and differentiation, the 3D-printed PGS framework reduced risks of cell-mediated contraction,

thereby ensuring a greater surface area available to the cells. Consequently, this may have translated into enhanced MSC migration, proliferation, and matrix deposition in composite scaffolds. Furthermore, the gene expression of collagen type II (a typical gene associated with successful MSC chondrogenesis[53]) was also upregulated in the differentiated MSCs colonizing the composite scaffold when compared to other groups. This indicates that the composite scaffold exhibits a strong ability to direct higher-quality MSC chondrogenic differentiation. Interestingly, the more restricted structure of the collagen-based matrix in the composite scaffold due to the PGS framework mediates an effect that may affect MSC behaviour and SOX9 (a key early promoter) through the ROCK pathway. It is possible that higher tensional forces on the cell's cytoskeleton due to the PGS filaments activate ROCK, which in turn phosphorylates SOX9, determining its activation and pro-chondrogenic effect [54,55]. Further investigation on the cell-mechanic signal effects induced by the combination of the 3D-printed PGS framework and the pro-chondrogenic CI/II-HyA matrix can be conducted. Taken together, the overall results of this study are sufficient to demonstrate that collagen-based PGS composite scaffold is an excellent biomimetic scaffold with a strong possibility to succeed *in vivo* in enhancing cartilage defect repair.

In the end, this study has demonstrated the significant potential of collagen-based PGS composite scaffolds for cartilage defect repair, regarding architecture, mechanical properties, degradation, and MSC chondrogenesis. However, there are still some limitations. Firstly, cartilage, especially articular cartilage, is frequently exposed to complex stress environments *in vivo* due to the host movements, including unstable compression and shear forces. This study only tested mechanical properties under stable compression, lacking investigations into long-term fatigue behaviour under more complex, unstable stress conditions. Additionally, investigations on *in vivo* degradation and *in vivo* chondrogenesis of tissue-engineered cartilage implants are critical for assessing their clinical potential. Future research will focus on implanting the composite scaffolds into animal articular cartilage models to monitor and record degradation behaviour and cartilage regeneration over time. Furthermore, composite scaffolds loaded with mesenchymal stem cells will also be implanted to explore potential synergistic effects, in order to further enhance the cartilage defect repair efficiency for clinical applications.

Conclusion

In this study, a novel biomimetic collagen-based 3D-printed PGS composite scaffold was specifically designed to enhance cartilage defect repair, whereby the porous CI/II-HyA matrix served as the biological cue for MSC chondrogenic stimulation and the PGS scaffold as the mechanical enforcement to support tissue growth. The resulting composite scaffold exhibited mechanical properties similar to native cartilage, promoting accurate MSC differentiation and abundant cartilage-like matrix deposition at 28 days *in vitro*,

while maintaining structural, mass, and mechanical stability during the initial cartilage regeneration period of 4 weeks. Taken together, this novel biomimetic composite scaffold with adaptive properties to native tissue holds great promise as an attractive “off-the-shelf” alternative clinical approach in cartilage tissue engineering.

Acknowledgements

This work was supported by the Spanish Research Agency through the grant PID2021-124389OB-C21 and the European Research Council (ERC) Advanced Grant n°788753 (ReCaP). Ms. Y. Liu acknowledges the support from the China Scholarship Council (CSC No. 202106990026).

Reference

[1] X. Yan, B. Yang, Y. Chen, Y. Song, J. Ye, Y. Pan, B. Zhou, Y. Wang, F. Mao, Y. Dong, D. Liu, J. Yu, Anti-Friction MSCs Delivery System Improves the Therapy for Severe Osteoarthritis, Advanced Materials 33 (2021). https://doi.org/10.1002/adma.202104758.

[2] M.K. Mamidi, A.K. Das, Z. Zakaria, R. Bhonde, Mesenchymal stromal cells for cartilage repair in osteoarthritis, Osteoarthritis Cartilage 24 (2016) 1307–1316. https://doi.org/10.1016/j.joca.2016.03.003.

[3] S. Camarero-Espinosa, B. Rothen-Rutishauser, E.J. Foster, C. Weder, Articular cartilage: From formation to tissue engineering, Biomater Sci 4 (2016) 734–767. https://doi.org/10.1039/c6bm00068a.

[4] Z.H. Deng, Y.S. Li, X. Gao, G.H. Lei, J. Huard, Bone morphogenetic proteins for articular cartilage regeneration, Osteoarthritis Cartilage 26 (2018) 1153–1161. https://doi.org/10.1016/j.joca.2018.03.007.

[5] J.M. Patel, K.S. Saleh, J.A. Burdick, R.L. Mauck, Bioactive factors for cartilage repair and regeneration: Improving delivery, retention, and activity, Acta Biomater 93 (2019) 222–238. https://doi.org/10.1016/j.actbio.2019.01.061.

[6] D. Gonzalez-Rodriguez, K. Guevorkian, S. Douezan, F. Brochard-Wyart, Soft matter models of developing tissues and tumors, Science (1979) 338 (2012) 910–917. https://doi.org/10.1126/science.1226418.

[7] X. Nie, Y.J. Chuah, W. Zhu, P. He, Y. Peck, D.A. Wang, Decellularized tissue engineered hyaline cartilage graft for articular cartilage repair, Biomaterials 235 (2020). https://doi.org/10.1016/j.biomaterials.2020.119821.

[8] F. Migliorini, N. Maffulli, A. Baroncini, J. Eschweiler, M. Knobe, M. Tingart, H. Schenker, Allograft Versus Autograft Osteochondral Transplant for Chondral Defects of the Talus: Systematic Review and Meta-analysis, American Journal of Sports Medicine 50 (2022) 3447–3455. https://doi.org/10.1177/03635465211037349.

[9] A. Maihemuti, H. Zhang, X. Lin, Y. Wang, Z. Xu, D. Zhang, Q. Jiang, 3D-printed fish gelatin scaffolds for cartilage tissue engineering, Bioact Mater 26 (2023) 77–87. https://doi.org/10.1016/j.bioactmat.2023.02.007.

[10] P. Li, L. Fu, Z. Liao, Y. Peng, C. Ning, C. Gao, D. Zhang, X. Sui, Y. Lin, S. Liu, C. Hao, Q. Guo, Chitosan hydrogel/3D-printed poly(ε-caprolactone) hybrid scaffold containing synovial mesenchymal stem cells for cartilage regeneration based on tetrahedral framework nucleic acid recruitment, Biomaterials 278 (2021). https://doi.org/10.1016/j.biomaterials.2021.121131.

[11] W. Wei, H. Dai, Articular cartilage and osteochondral tissue engineering techniques: Recent advances and challenges, Bioact Mater 6 (2021) 4830–4855. https://doi.org/10.1016/j.bioactmat.2021.05.011.

[12] S. Wang, S. Zhao, J. Yu, Z. Gu, Y. Zhang, Advances in Translational 3D Printing for Cartilage, Bone, and Osteochondral Tissue Engineering, Small 18 (2022). https://doi.org/10.1002/smll.202201869.

[13] B.A.G. de Melo, Y.A. Jodat, S. Mehrotra, M.A. Calabrese, T. Kamperman, B.B. Mandal, M.H.A. Santana, E. Alsberg, J. Leijten, S.R. Shin, 3D Printed Cartilage-Like Tissue Constructs with Spatially Controlled Mechanical Properties, Adv Funct Mater 29 (2019). https://doi.org/10.1002/adfm.201906330.

[14] Y.Y. Liu, J.P.F. Blazquez, G.Z. Yin, D.Y. Wang, J. Llorca, M. Echeverry-Rendón, A strategy to tailor the mechanical and degradation properties of PCL-PEG-PCL based

copolymers for biomedical application, Eur Polym J 198 (2023). https://doi.org/10.1016/j.eurpolymj.2023.112388.
[15] Y. Cao, P. Cheng, S. Sang, C. Xiang, Y. An, X. Wei, Y. Yan, P. Li, 3D printed PCL/GelMA biphasic scaffold boosts cartilage regeneration using co-culture of mesenchymal stem cells and chondrocytes: In vivo study, Mater Des 210 (2021). https://doi.org/10.1016/j.matdes.2021.110065.
[16] X. Gui, Z. Peng, P. Song, L. Chen, X. Xu, H. Li, P. Tang, Y. Wang, Z. Su, Q. Kong, Z. Zhang, Z. Li, Y. Cen, C. Zhou, Y. Fan, X. Zhang, 3D printing of personalized polylactic acid scaffold laden with GelMA/autologous auricle cartilage to promote ear reconstruction, Biodes Manuf 6 (2023) 451–463. https://doi.org/10.1007/s42242-023-00242-6.
[17] Y. Tang, H. Wang, Y. Sun, Y. Jiang, S. Fang, Z. Kan, Y. Lu, S. Liu, X. Zhou, Z. Li, Using Platelet-Rich Plasma Hydrogel to Deliver Mesenchymal Stem Cells into Three-Dimensional PLGA Scaffold for Cartilage Tissue Engineering, ACS Appl Bio Mater 4 (2021) 8607–8614. https://doi.org/10.1021/acsabm.1c01160.
[18] L. Vogt, F. Ruther, S. Salehi, A.R. Boccaccini, Poly(Glycerol Sebacate) in Biomedical Applications—A Review of the Recent Literature, Adv Healthc Mater 10 (2021). https://doi.org/10.1002/adhm.202002026.
[19] D. Lei, Y. Yang, Z. Liu, S. Chen, B. Song, A. Shen, B. Yang, S. Li, Z. Yuan, Q. Qi, L. Sun, Y. Guo, H. Zuo, S. Huang, Q. Yang, X. Mo, C. He, B. Zhu, E.M. Jeffries, F.L. Qing, X. Ye, Q. Zhao, Z. You, A general strategy of 3D printing thermosets for diverse applications, Mater Horiz 6 (2019) 394–404. https://doi.org/10.1039/c8mh00937f.
[20] S. Huang, D. Lei, Q. Yang, Y. Yang, C. Jiang, H. Shi, B. Qian, Q. Long, W. Chen, Y. Chen, L. Zhu, W. Yang, L. Wang, W. Hai, Q. Zhao, Z. You, X. Ye, A perfusable, multifunctional epicardial device improves cardiac function and tissue repair, Nat Med 27 (2021) 480–490. https://doi.org/10.1038/s41591-021-01279-9.
[21] Y. Yang, D. Lei, S. Huang, Q. Yang, B. Song, Y. Guo, A. Shen, Z. Yuan, S. Li, F.L. Qing, X. Ye, Z. You, Q. Zhao, Elastic 3D-Printed Hybrid Polymeric Scaffold Improves Cardiac Remodeling after Myocardial Infarction, Adv Healthc Mater 8 (2019). https://doi.org/10.1002/adhm.201900065.
[22] S. Wang, H. Chen, J. Huang, S. Shen, Z. Tang, X. Tan, D. Lei, G. Zhou, Gelatin-modified 3D printed PGS elastic hierarchical porous scaffold for cartilage regeneration, APL Bioeng 7 (2023). https://doi.org/10.1063/5.0152151.
[23] S. Wang, B. Luo, B. Bai, Q. Wang, H. Chen, X. Tan, Z. Tang, S. Shen, H. Zhou, Z. You, G. Zhou, D. Lei, 3D Printed Chondrogenic Functionalized PGS Bioactive Scaffold for Cartilage Regeneration, Adv Healthc Mater 12 (2023). https://doi.org/10.1002/adhm.202301006.
[24] M. Chen, Y.Y. Li, S. Liu, Z. Feng, H. Wang, D. Yang, W. Guo, Z. Yuan, S. Gao, Y. Zhang, K. Zha, B. Huang, F. Wei, X. Sang, Q. Tian, X. Yang, X. sui, Y. Zhou, Y. Zheng, Q. Guo, Hierarchical macro-microporous WPU-ECM scaffolds combined with Microfracture Promote in Situ Articular Cartilage Regeneration in Rabbits, Bioact Mater 6 (2021) 1932–1944. https://doi.org/10.1016/j.bioactmat.2020.12.009.
[25] Z. Yang, T. Zhao, C. Gao, F. Cao, H. Li, Z. Liao, L. Fu, P. Li, W. Chen, Z. Sun, S. Jiang, Z. Tian, G. Tian, K. Zha, T. Pan, X. Li, X. Sui, Z. Yuan, S. Liu, Q. Guo, 3D-Bioprinted Difunctional Scaffold for in Situ Cartilage Regeneration Based on Aptamer-Directed Cell

Recruitment and Growth Factor-Enhanced Cell Chondrogenesis, ACS Appl Mater Interfaces 13 (2021) 23369–23383. https://doi.org/10.1021/acsami.1c01844.
[26] M. Joyce, T. Hodgkinson, C. Intini, J. Dixon, D. Kelly, F. O'Brien, Gene activated reinforced scaffolds for SOX9 delivery to enhance repair of large load bearing articular cartilage defects, Eur Cell Mater 47 (2024) 91–108. https://doi.org/10.22203/ecm.v047a07.
[27] P. Salahshour, NANOBIOMATERIALS/BIOINKS BASED SCAFFOLDS IN 3D BIOPRINTING FOR TISSUE ENGINEERING AND ARTIFICIAL HUMAN ORGANS, Advances in Biology & Earth Sciences 9 (2024) 97–104. https://doi.org/10.62476/abes9s97.
[28] A. Kirillova, T.R. Yeazel, D. Asheghali, S.R. Petersen, S. Dort, K. Gall, M.L. Becker, Fabrication of Biomedical Scaffolds Using Biodegradable Polymers, Chem Rev 121 (2021) 11238–11304. https://doi.org/10.1021/acs.chemrev.0c01200.
[29] F. Zhang, M.W. King, Biodegradable Polymers as the Pivotal Player in the Design of Tissue Engineering Scaffolds, Adv Healthc Mater 9 (2020). https://doi.org/10.1002/adhm.201901358.
[30] T.J. Levingstone, A. Matsiko, G.R. Dickson, F.J. O'Brien, J.P. Gleeson, A biomimetic multi-layered collagen-based scaffold for osteochondral repair, Acta Biomater 10 (2014) 1996–2004. https://doi.org/10.1016/j.actbio.2014.01.005.
[31] E. Ahmadian, A. Eftekhari, D. Janas, P. Vahedi, Nanofiber scaffolds based on extracellular matrix for articular cartilage engineering: A perspective, Nanotheranostics 7 (2023) 61–69. https://doi.org/10.7150/ntno.78611.
[32] C. Intini, T. Hodgkinson, S.M. Casey, J.P. Gleeson, F.J. O'brien, Highly Porous Type II Collagen-Containing Scaffolds for Enhanced Cartilage Repair with Reduced Hypertrophic Cartilage Formation, Bioengineering 9 (2022). https://doi.org/10.3390/bioengineering9060232.
[33] C. Intini, M. Lemoine, T. Hodgkinson, S. Casey, J.P. Gleeson, F.J. O'Brien, A highly porous type II collagen containing scaffold for the treatment of cartilage defects enhances MSC chondrogenesis and early cartilaginous matrix deposition, Biomater Sci 10 (2022) 970–983. https://doi.org/10.1039/d1bm01417j.
[34] T.J. Levingstone, E. Thompson, A. Matsiko, A. Schepens, J.P. Gleeson, F.J. O'brien, Multi-layered collagen-based scaffolds for osteochondral defect repair in rabbits, Acta Biomater 32 (2016) 149–160. https://doi.org/10.1016/j.actbio.2015.12.034.
[35] T.J. Levingstone, A. Ramesh, R.T. Brady, P.A.J. Brama, C. Kearney, J.P. Gleeson, F.J. O'Brien, Cell-free multi-layered collagen-based scaffolds demonstrate layer specific regeneration of functional osteochondral tissue in caprine joints, Biomaterials 87 (2016) 69–81. https://doi.org/10.1016/j.biomaterials.2016.02.006.
[36] J.D. Stack, T.J. Levingstone, W. Lalor, R. Sanders, C. Kearney, F.J. O'Brien, F. David, Repair of large osteochondritis dissecans lesions using a novel multilayered tissue engineered construct in an equine athlete, J Tissue Eng Regen Med 11 (2017) 2785–2795. https://doi.org/https://doi.org/10.1002/term.2173.
[37] M.G. Haugh, C.M. Murphy, F.J. O'Brien, Novel Freeze-Drying Methods to Produce a Range of Collagen–Glycosaminoglycan Scaffolds with Tailored Mean Pore Sizes, Tissue Eng Part C Methods 16 (2009) 887–894. https://doi.org/10.1089/ten.tec.2009.0422.
[38] Implants for surgery-Homopolymers, copolymers and blends on poly(lactide)-In vitro degradation testing Implants chirurgicaux-Homopolymères, copolymères et mélanges sur

poly(lactide)-Essais de dégradation in vitro COPYRIGHT PROTECTED DOCUMENT, 2017. www.iso.org.
[39] R.M. Raftery, E.G. Tierney, C.M. Curtin, S.A. Cryan, F.J. O'Brien, Development of a gene-activated scaffold platform for tissue engineering applications using chitosan-pDNA nanoparticles on collagen-based scaffolds, Journal of Controlled Release 210 (2015) 84–94. https://doi.org/10.1016/j.jconrel.2015.05.005.
[40] C. Intini, L.B. Ferreras, S. Casey, J.E. Dixon, J.P. Gleeson, F.J. O'Brien, An Innovative miR-Activated Scaffold for the Delivery of a miR-221 Inhibitor to Enhance Cartilage Defect Repair, Adv Ther (Weinh) 6 (2023). https://doi.org/10.1002/adtp.202200329.
[41] C.M. Murphy, M.G. Haugh, F.J. O'Brien, The effect of mean pore size on cell attachment, proliferation and migration in collagen-glycosaminoglycan scaffolds for bone tissue engineering, Biomaterials 31 (2010) 461–466. https://doi.org/10.1016/j.biomaterials.2009.09.063.
[42] J. Eschweiler, N. Horn, B. Rath, M. Betsch, A. Baroncini, M. Tingart, F. Migliorini, The biomechanics of cartilage-an overview, Life 11 (2021). https://doi.org/10.3390/life11040302.
[43] A. Matsiko, J.P. Gleeson, F.J. O'Brien, Scaffold Mean Pore Size Influences Mesenchymal Stem Cell Chondrogenic Differentiation and Matrix Deposition, Tissue Eng Part A 21 (2014) 486–497. https://doi.org/10.1089/ten.tea.2013.0545.
[44] H. Chen, G. Gonnella, J. Huang, L. Di-Silvio, Fabrication of 3D Bioprinted Bi-Phasic Scaffold for Bone–Cartilage Interface Regeneration, Biomimetics 8 (2023). https://doi.org/10.3390/biomimetics8010087.
[45] C.H. Chen, C.Y. Kuo, J.P. Chen, Effect of cyclic dynamic compressive loading on chondrocytes and adipose-derived stem cells co-cultured in highly elastic cryogel scaffolds, Int J Mol Sci 19 (2018). https://doi.org/10.3390/ijms19020370.
[46] J.T. Bingham, R. Papannagari, S.K. Van de velde, C. Gross, T.J. Gill, D.T. Felson, H.E. Rubash, G. Li, In vivo cartilage contact deformation in the healthy human tibiofemoral joint, Rheumatology 47 (2008) 1622–1627. https://doi.org/10.1093/rheumatology/ken345.
[47] C. Herberhold, S. Faber, T. Stammberger, M. Steinlechner, R. Putz, K.H. Englmeier, M. Reiser, F. Eckstein, In situ measurement of articular cartilage deformation in intact femoropatellar joints under static loading, 1999.
[48] W.Y. Lin, Y.H. Chang, H.Y. Wang, T.C. Yang, T.K. Chiu, S. Bin Huang, M.H. Wu, The study of the frequency effect of dynamic compressive loading on primary articular chondrocyte functions using a microcell culture system, Biomed Res Int 2014 (2014). https://doi.org/10.1155/2014/762570.
[49] S. Camarero-Espinosa, A. Calore, A. Wilbers, J. Harings, L. Moroni, Additive manufacturing of an elastic poly(ester)urethane for cartilage tissue engineering, Acta Biomater 102 (2020) 192–204. https://doi.org/10.1016/j.actbio.2019.11.041.
[50] Y. Liu, K. Tian, J. Hao, T. Yang, X. Geng, W. Zhang, Biomimetic poly(glycerol sebacate)/polycaprolactone blend scaffolds for cartilage tissue engineering, J Mater Sci Mater Med 30 (2019). https://doi.org/10.1007/s10856-019-6257-3.
[51] S. Critchley, E.J. Sheehy, G. Cunniffe, P. Diaz-Payno, S.F. Carroll, O. Jeon, E. Alsberg, P.A.J. Brama, D.J. Kelly, 3D printing of fibre-reinforced cartilaginous templates for the regeneration of osteochondral defects, Acta Biomater 113 (2020) 130–143. https://doi.org/10.1016/j.actbio.2020.05.040.

[52] J. Hauptstein, T. Böck, M. Bartolf-Kopp, L. Forster, P. Stahlhut, A. Nadernezhad, G. Blahetek, A. Zernecke-Madsen, R. Detsch, T. Jüngst, J. Groll, J. Teßmar, T. Blunk, Hyaluronic Acid-Based Bioink Composition Enabling 3D Bioprinting and Improving Quality of Deposited Cartilaginous Extracellular Matrix, Adv Healthc Mater 9 (2020). https://doi.org/10.1002/adhm.202000737.
[53] M.B. Goldring, Chondrogenesis, chondrocyte differentiation, and articular cartilage metabolism in health and osteoarthritis, Ther Adv Musculoskelet Dis 4 (2012) 269–285. https://doi.org/10.1177/1759720X12448454.
[54] A. Woods, G. Wang, F. Beier, RhoA/ROCK signaling regulates Sox9 expression and actin organization during chondrogenesis, Journal of Biological Chemistry 280 (2005) 11626–11634. https://doi.org/10.1074/jbc.M409158200.
[55] D.R. Haudenschild, J. Chen, N. Pang, M.K. Lotz, D.D. D'Lima, Rho kinase-dependent activation of SOX9 in chondrocytes, Arthritis Rheum 62 (2010) 191–200. https://doi.org/10.1002/art.25051.